

Supported in part by



Highlights from STAR beam energy scan II program

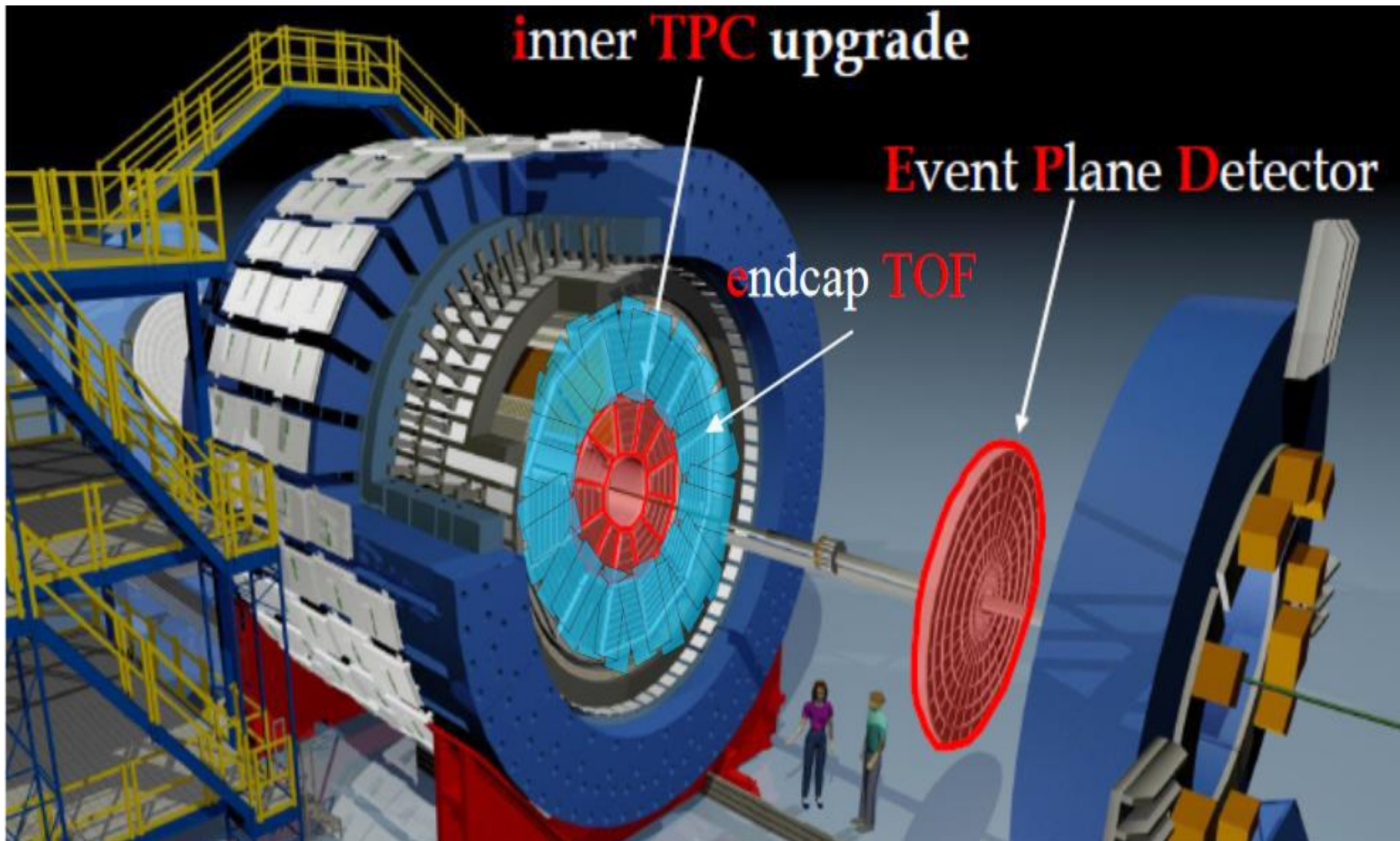
Alexey Aparin for the STAR collaboration
Joint Institute for Nuclear Research



Part of this work has been supported by Russian Science Foundation under grant № 22-72-10028



STAR detector upgrades



- **Tracking and PID (full 2π)**
 - TPC: $|\eta| < 1$
 - iTPC (2019+): $|\eta| < 1.5$**
 - TOF: $|\eta| < 1$
 - eTOF (2019+): $-1.6 < \eta < -1$**
 - BEMC: $|\eta| < 1$
 - EEMC: $1 < \eta < 2$
 - HFT (2014-2016): $|\eta| < 1$
 - MTD (2014+): $|\eta| < 0.5$ (partial azimuthal coverage)
- **MB trigger and event plane reconstruction**
 - BBC (before 2018): $3.3 < |\eta| < 5$
 - EPD (2018+): $2.1 < |\eta| < 5.1$**
 - VPD: $4.2 < |\eta| < 5$
 - ZDC: $6.5 < |\eta| < 7.5$

Beam Energy Scan to map the QCD phase diagram



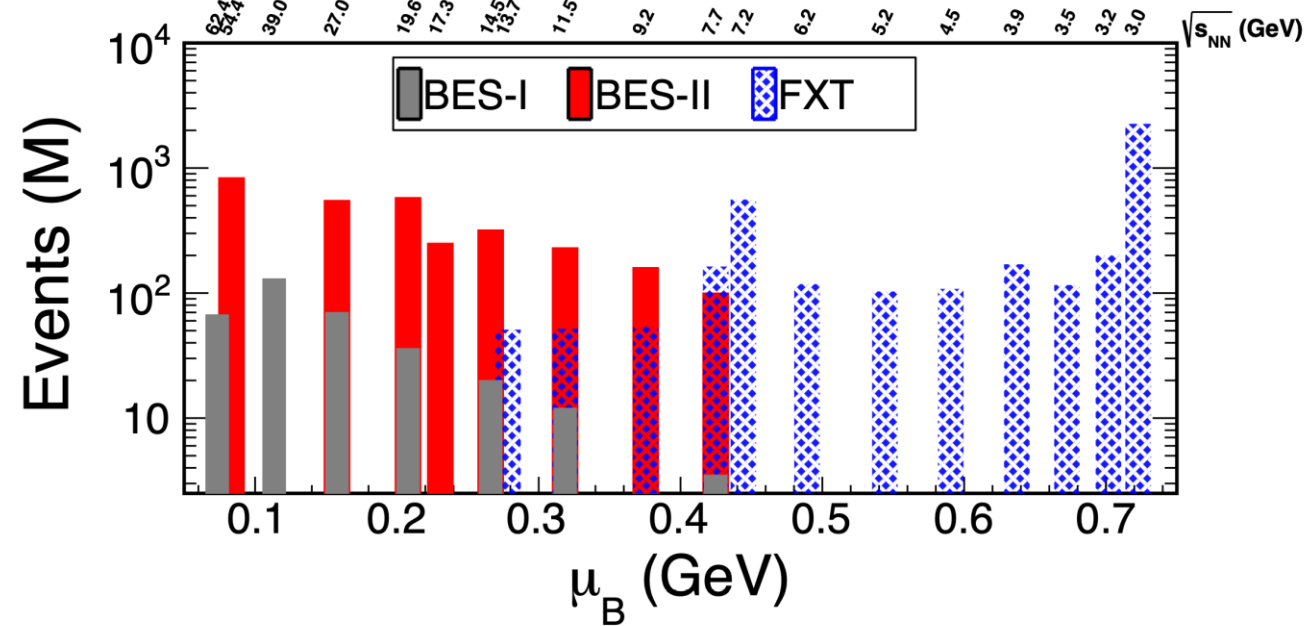
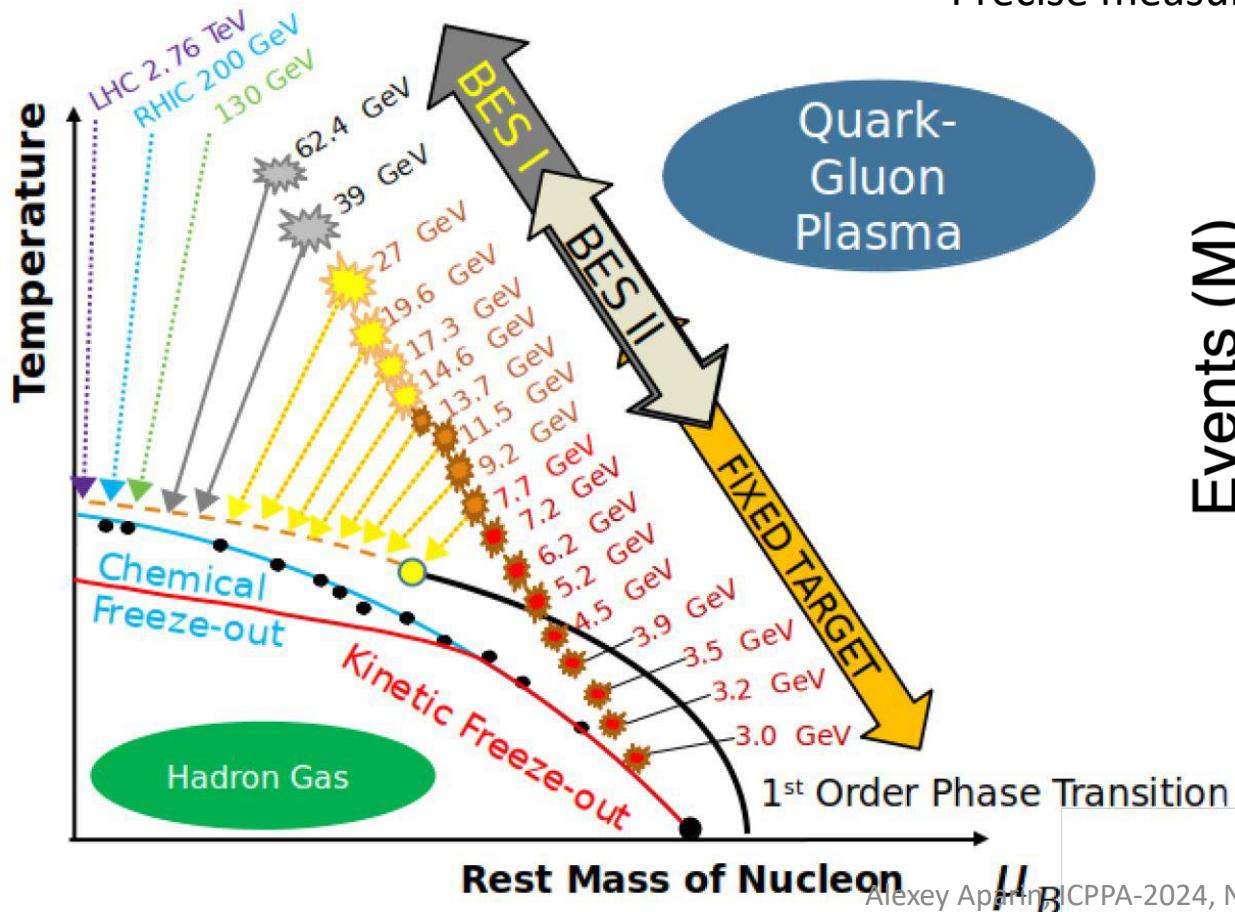
Two phases of Beam Energy Scan:

Phase I: 7.7 – 39 GeV 2010 – 2014

First glance at low energy region, rather low statistics

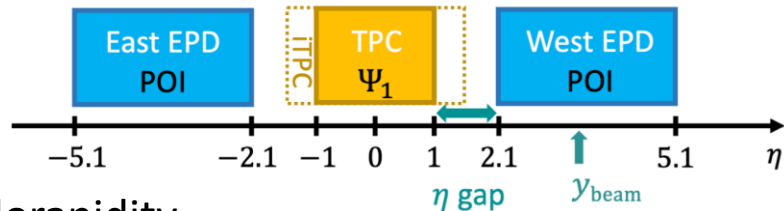
Phase II: 3 – 54.4 GeV 2017 – 2021

Precise measurements at low energies, large statistics



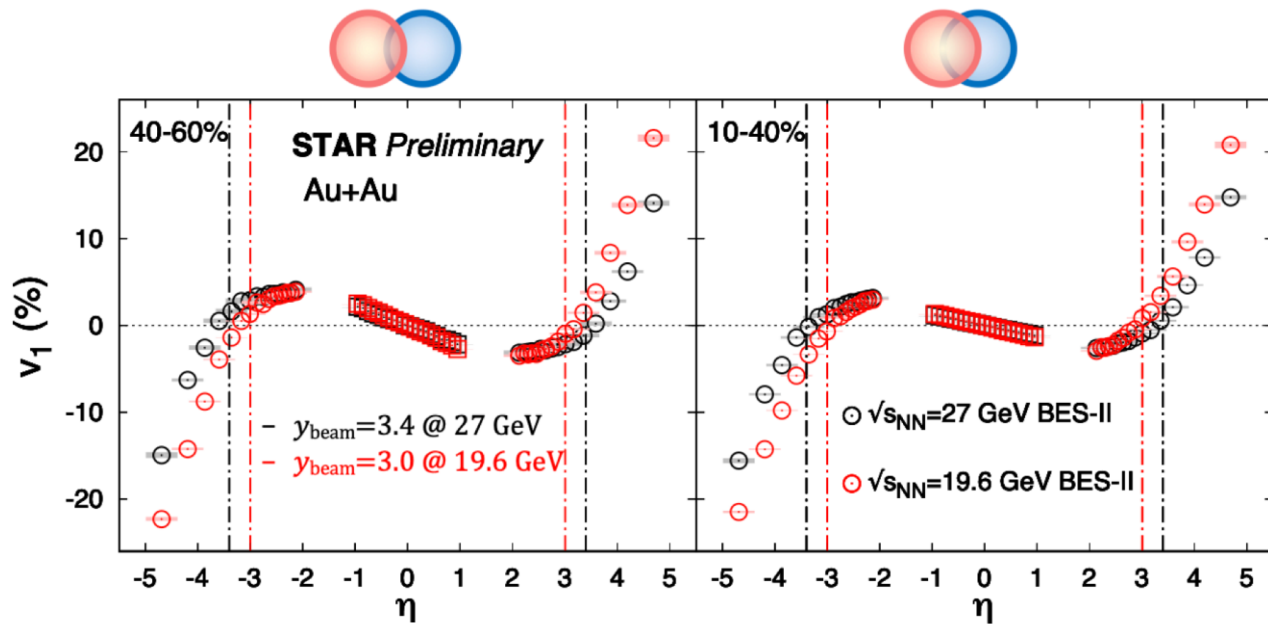
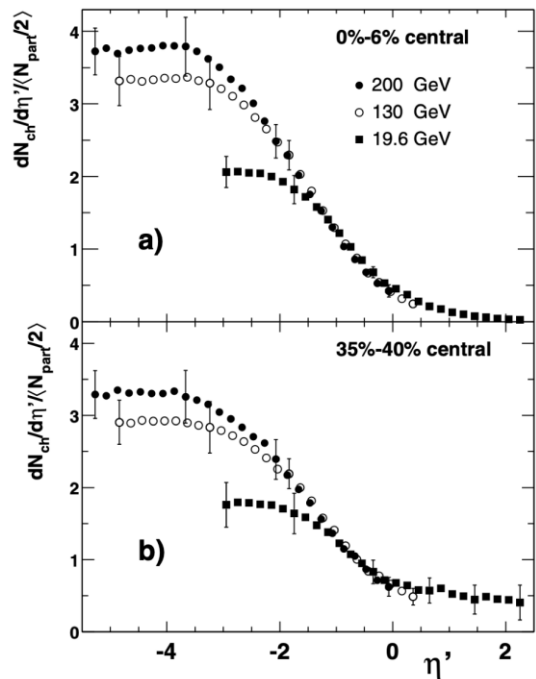
Measurements of rapidity dependence of flow

Symmetric reference

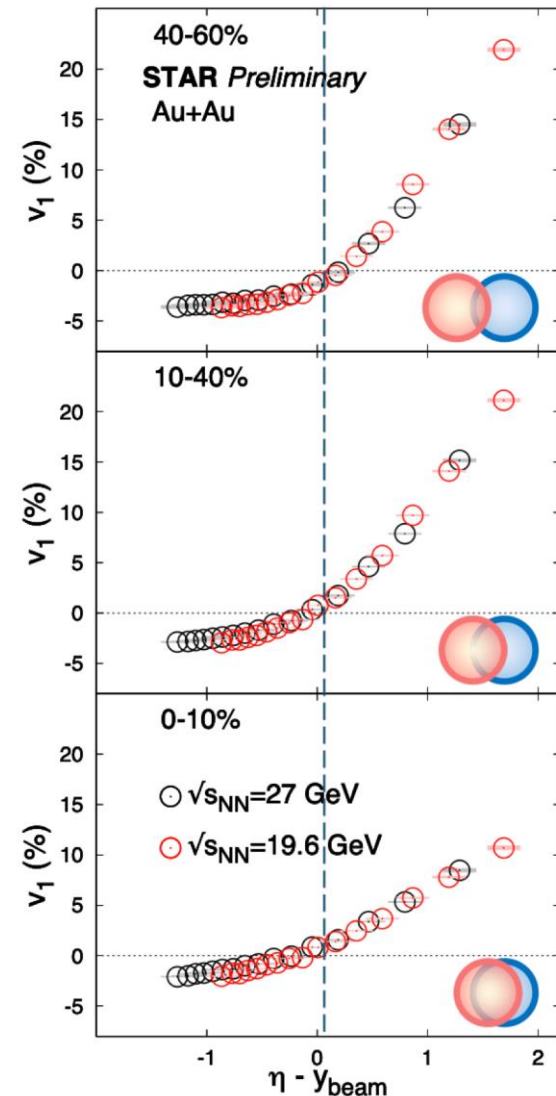


PHOBOS. PRL 91 (2003), 052303
 PHOBOS. PRL 97 (2006), 012301

Measurements of v_1 over 9 units of pseudorapidity



$$\frac{dN}{d\phi} \propto 1 + \sum_{n=1} 2v_n \cos n(\phi - \Psi_{RP})$$



Vast rapidity coverage allows to perform measurements of rapidity dependence of flow

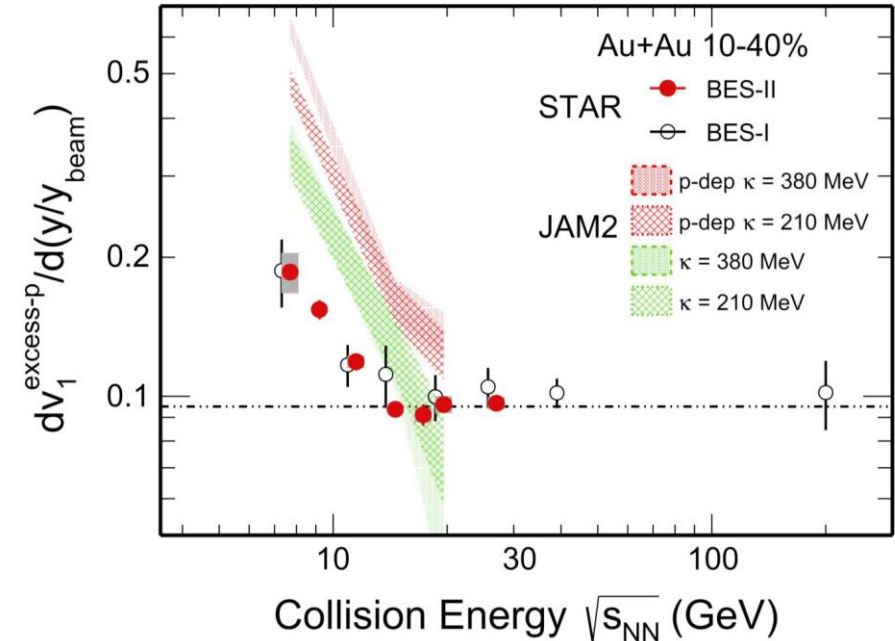
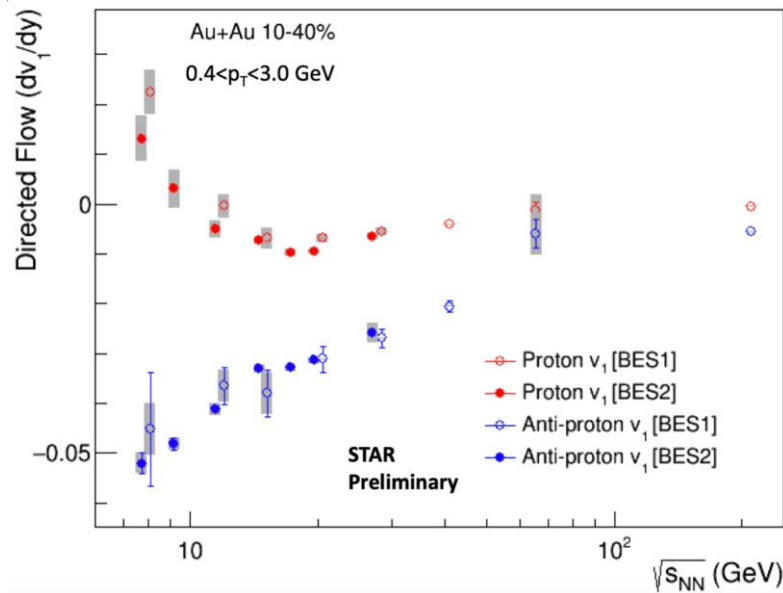
Observed limiting fragmentation of v_1 in Au+Au collisions at 19.6 and 27 GeV

Directed flow of protons and antiprotons

Directed flow of protons has two main sources:

Interaction between hadrons in the initial compression stages produces positive flow

Tilted matter produces negative flow during expansion stage



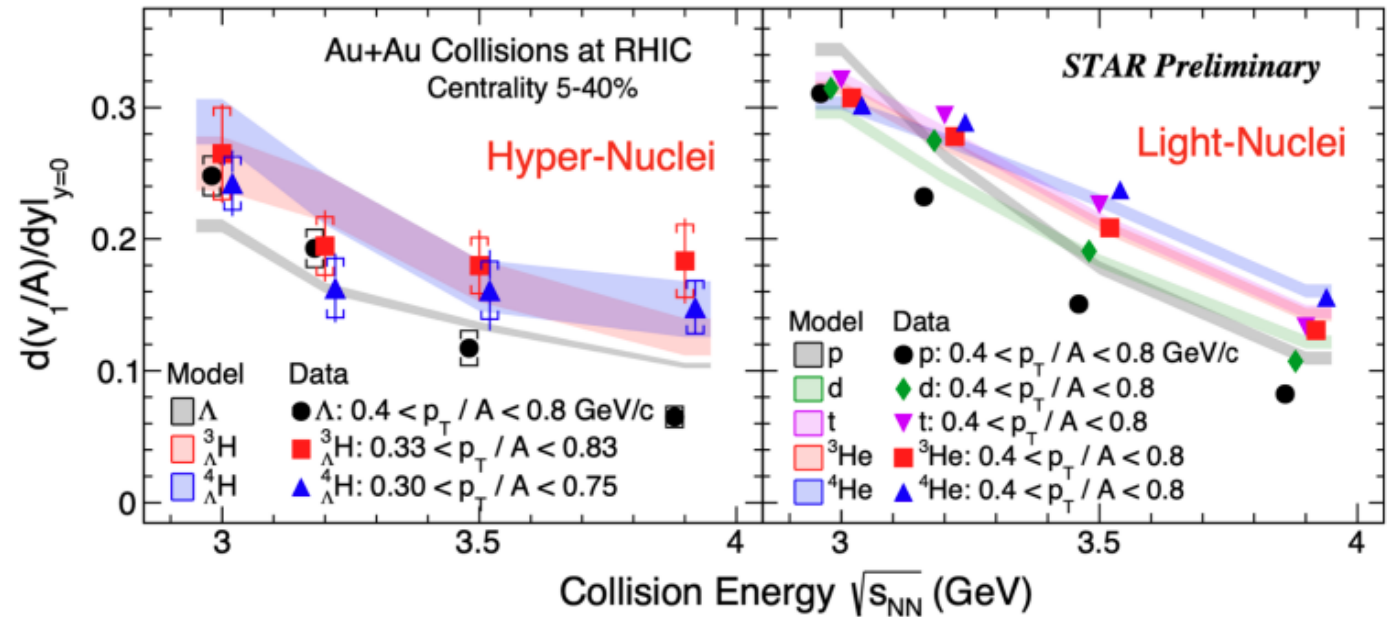
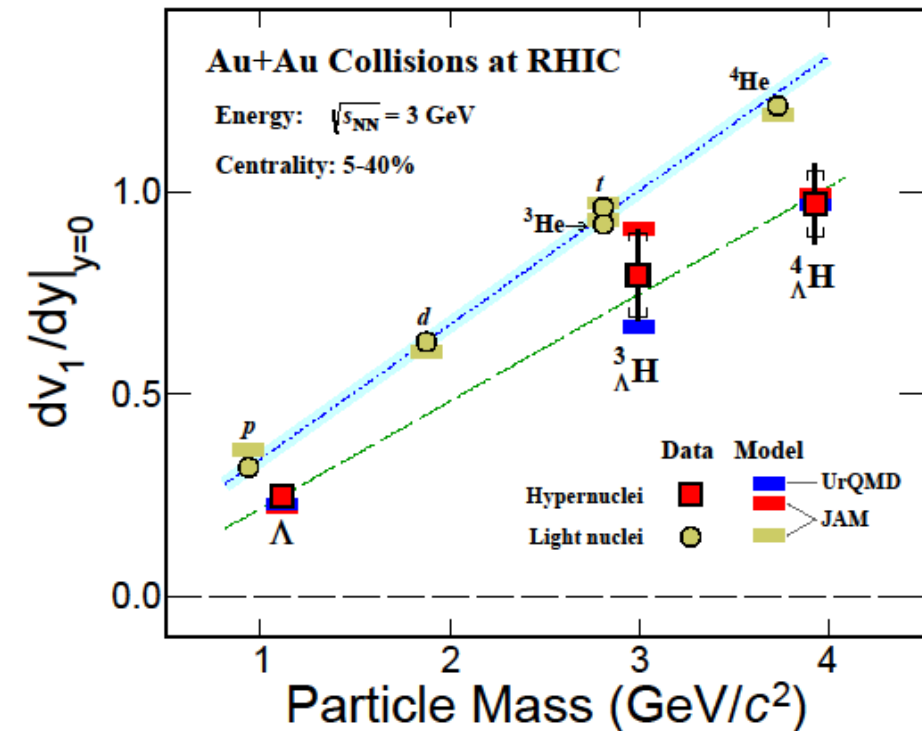
- Scaling of excess proton flow with collision energy
- Indication of scale breaking at 11.5 GeV a change in medium and collision dynamics
- Models fail to show the scaling behavior above 14.6 GeV

$$v_{1,\text{excess}} = \frac{(v_{1,p} - v_{1,\bar{p}})}{1-r}$$

r – is the yield ratio of antiprotons to protons

Directed flow of light and hyper nuclei

Mass ordering of v_1 is seen for light nuclei and hypernuclei. The slope parameter is different for hypernuclei.

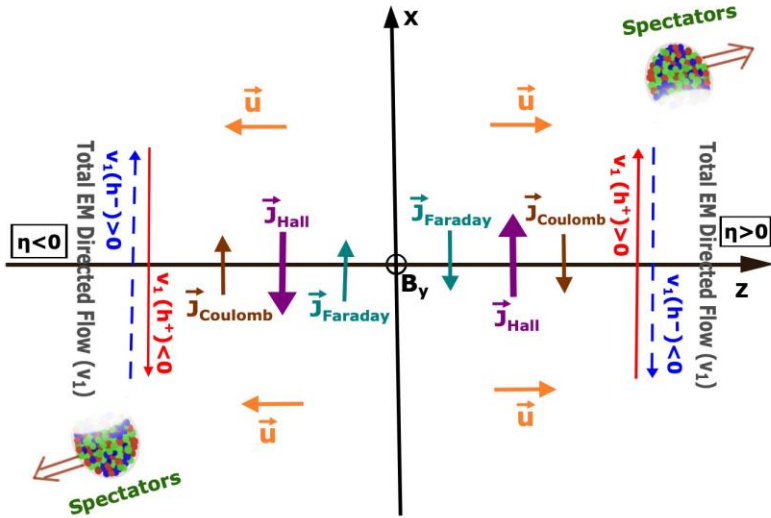


Slope parameter of v_1 decreases with the increase of collision energy

JAM2 mean field + coalescence calculations explains the energy dependence

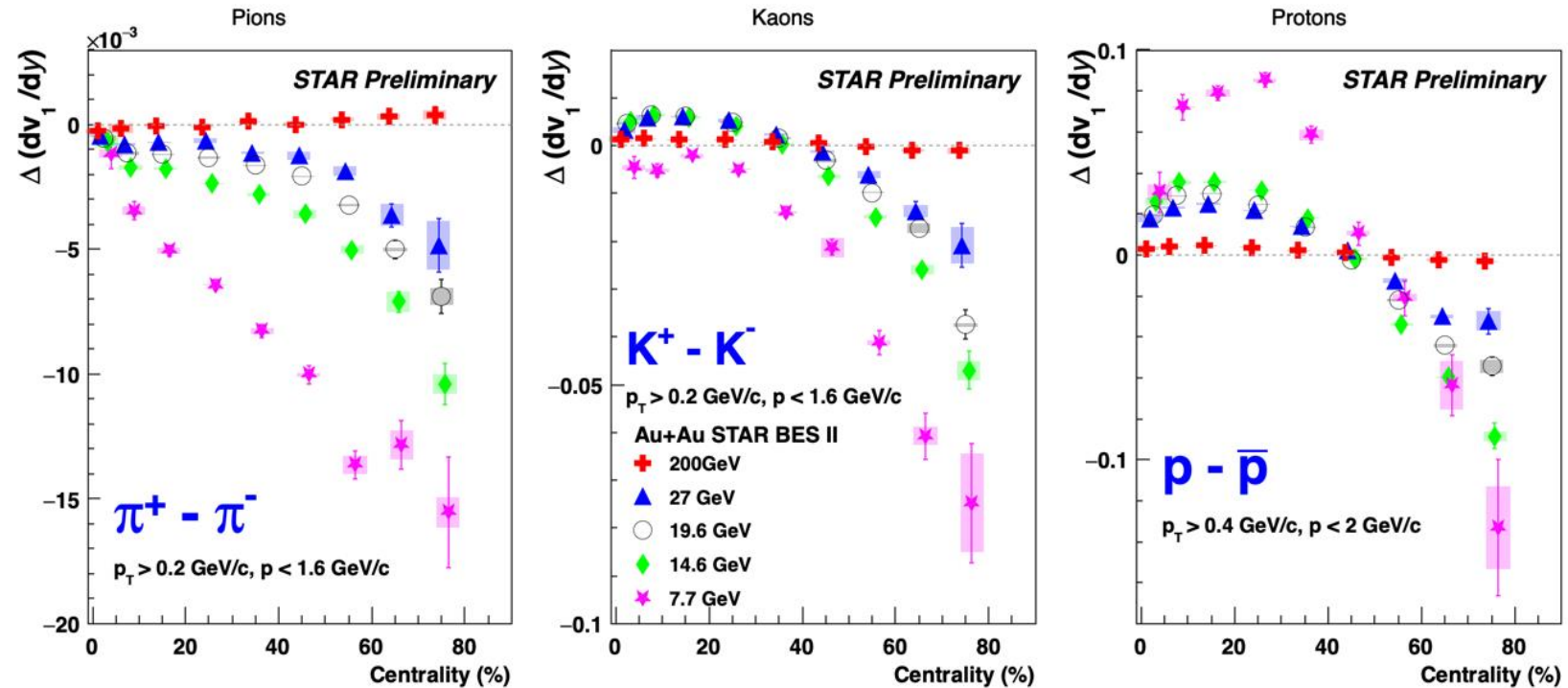
Directed flow splitting for charged particles

v_1 slope difference between particles and anti-particles is more negative at lower collision energies
 ➤ Could be due to EM-field effect, longer-lived field and shorter lifetime of fireball



Strong EM field from spectator protons can cause splitting of positively and negatively charged produced particles

v_1 splitting was previously obtained at high collision energies



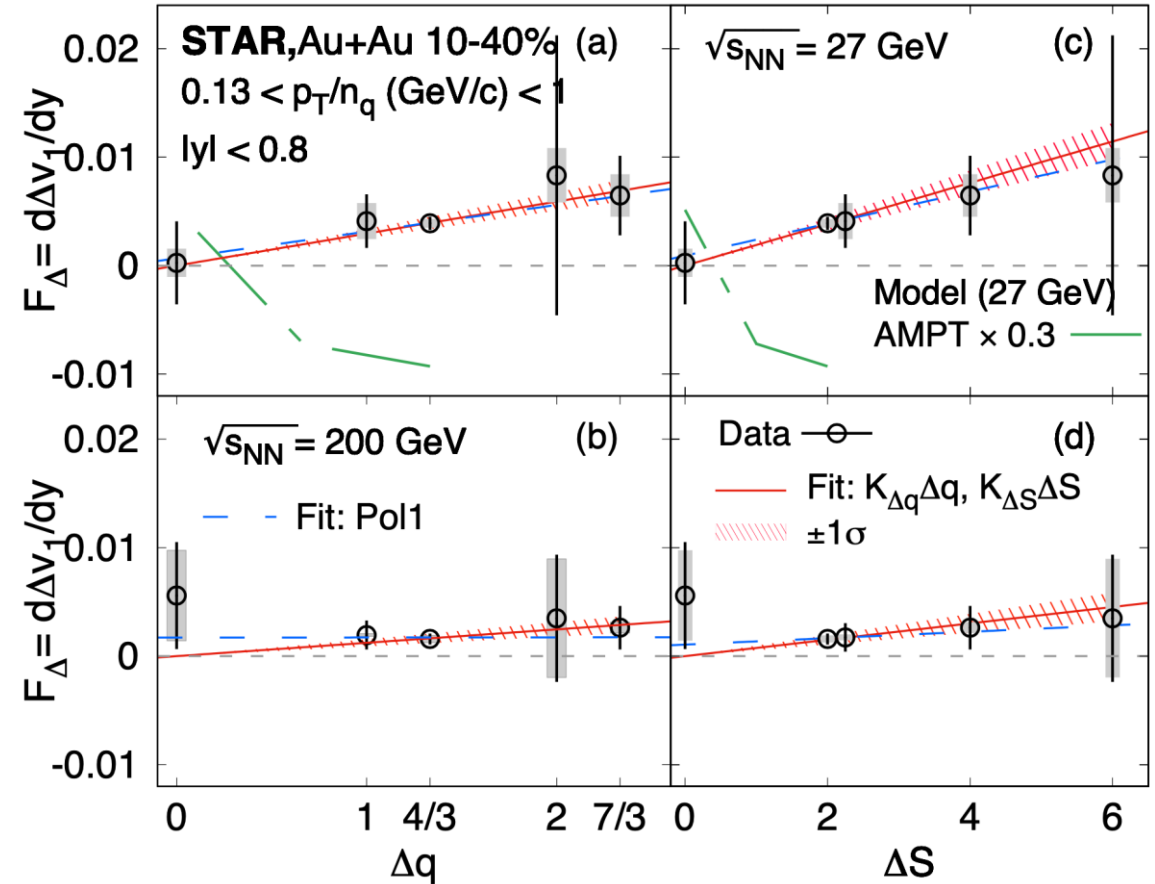
STAR, PRX 14 (2024), 011028
 U. Gursoy et al. PRC 98 (2018), 055201; PRC 89 (2014), 054905

Directed flow splitting for charged particles



Index	Quark Mass	Charge	Strangeness	Expression
1	$\Delta m = 0$	$\Delta q = 0$	$\Delta S = 0$	$[\bar{p}(\bar{u}\bar{u}\bar{d}) + \phi(s\bar{s})] - [K^-(\bar{u}s) + \bar{\Lambda}(\bar{u}\bar{d}\bar{s})]$
2	$\Delta m \approx 0$	$\Delta q = 1$	$\Delta S = 2$	$[\bar{\Lambda}(\bar{u}\bar{d}\bar{s})] - [\frac{1}{3}\Omega^-(sss) + \frac{2}{3}\bar{p}(\bar{u}\bar{u}\bar{d})]$
3	$\Delta m \approx 0$	$\Delta q = \frac{4}{3}$	$\Delta S = 2$	$[\bar{\Lambda}(\bar{u}\bar{d}\bar{s})] - [K^-(\bar{u}s) + \frac{1}{3}\bar{p}(\bar{u}\bar{u}\bar{d})]$
4	$\Delta m = 0$	$\Delta q = 2$	$\Delta S = 6$	$[\Omega^+(\bar{s}\bar{s}\bar{s})] - [\Omega^-(sss)]$
5	$\Delta m \approx 0$	$\Delta q = \frac{7}{3}$	$\Delta S = 4$	$[\Xi^+(\bar{d}\bar{s}\bar{s})] - [K^-(\bar{u}s) + \frac{1}{3}\Omega^-(sss)]$

- STAR has measured v_1 splitting for produced quarks in Au+Au collisions at 27 GeV and 200 GeV.
- Assuming coalescence, combinations of hadrons from produced quarks were used to investigate the charge and strangeness dependence.
- The results have shown a dependence on charge and strangeness for splitting.
- Splitting is larger at 27 GeV than at 200 GeV, and an AMPT model with no EM field fails to describe the measurements.



arXiv:2304.02831

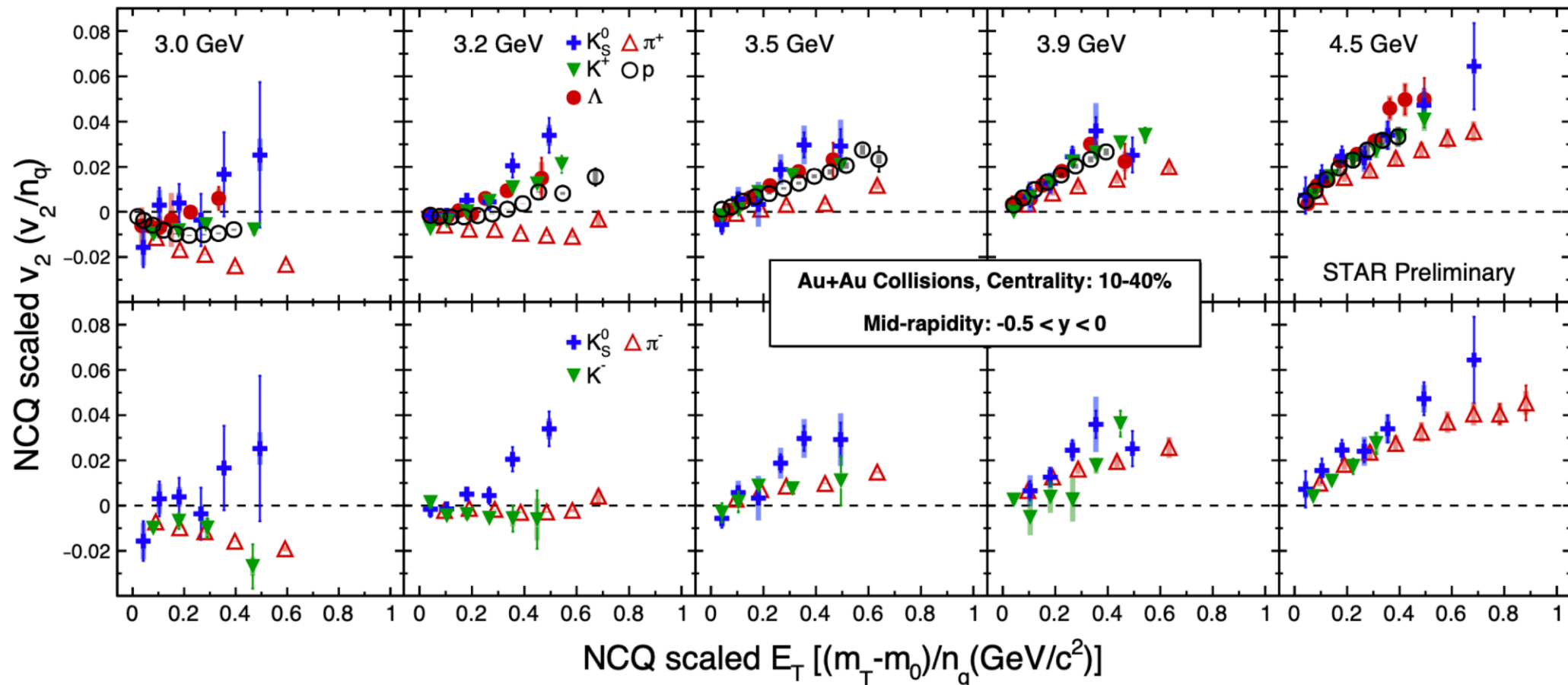
NCQ-scaling of v_2 at low energies

The quark number scaling has been used at higher energies as a signature of the QGP. At 3 and 3.2 GeV, the scaling is broken down.

Transition from pure hadronic to partonic interactions with the increase of the collision energy

Hadronic effects

Partonic effects





Cumulants of multiplicity distributions

Cumulants:

n = net-proton multiplicity
in an event

$$\delta n = n - \langle n \rangle$$

$$C_1 = \langle n \rangle$$

$$C_2 = \langle \delta n^2 \rangle$$

$$C_3 = \langle \delta n^3 \rangle$$

$$C_4 = \langle \delta n^4 \rangle - 3 \langle \delta n^2 \rangle^2$$

Factorial Cumulants:

$$\kappa_1 = C_1$$

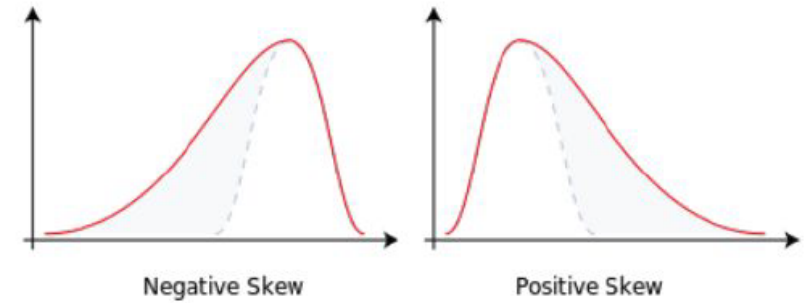
$$\kappa_2 = -C_1^2 + C_2$$

$$\kappa_3 = 2C_1 C_2 - 3C_3$$

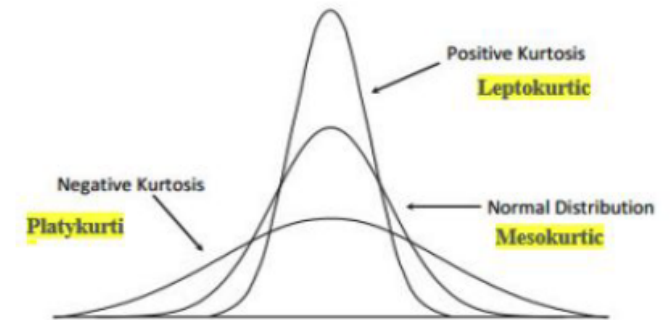
$$\kappa_4 = -6C_1 C_2 + 11C_2^2 - 6C_3 C_2 + C_4$$

Cumulants quantify characteristics of distributions:

Skewness: C_3/C_2

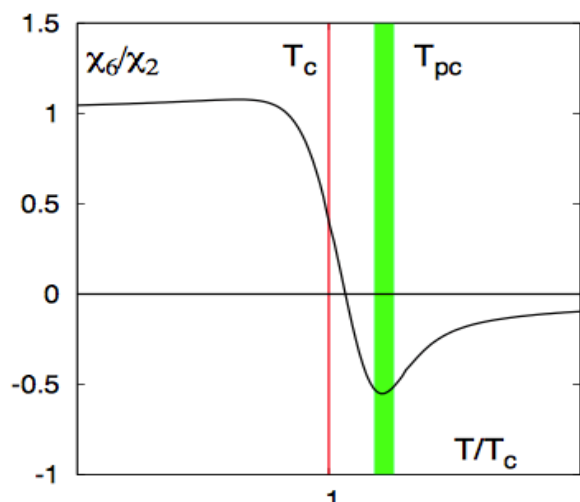


Kurtosis: C_4/C_2



Net-proton cumulant measurements at STAR

High order cumulants of conserved number distributions are sensitive to critical phenomena, related to the correlation length and susceptibilities.



Susceptibility ratios fluctuations near the CP

Cumulants

$$C_1 = \langle N \rangle$$

$$C_2 = \langle (\delta N)^2 \rangle$$

$$C_3 = \langle (\delta N)^3 \rangle$$

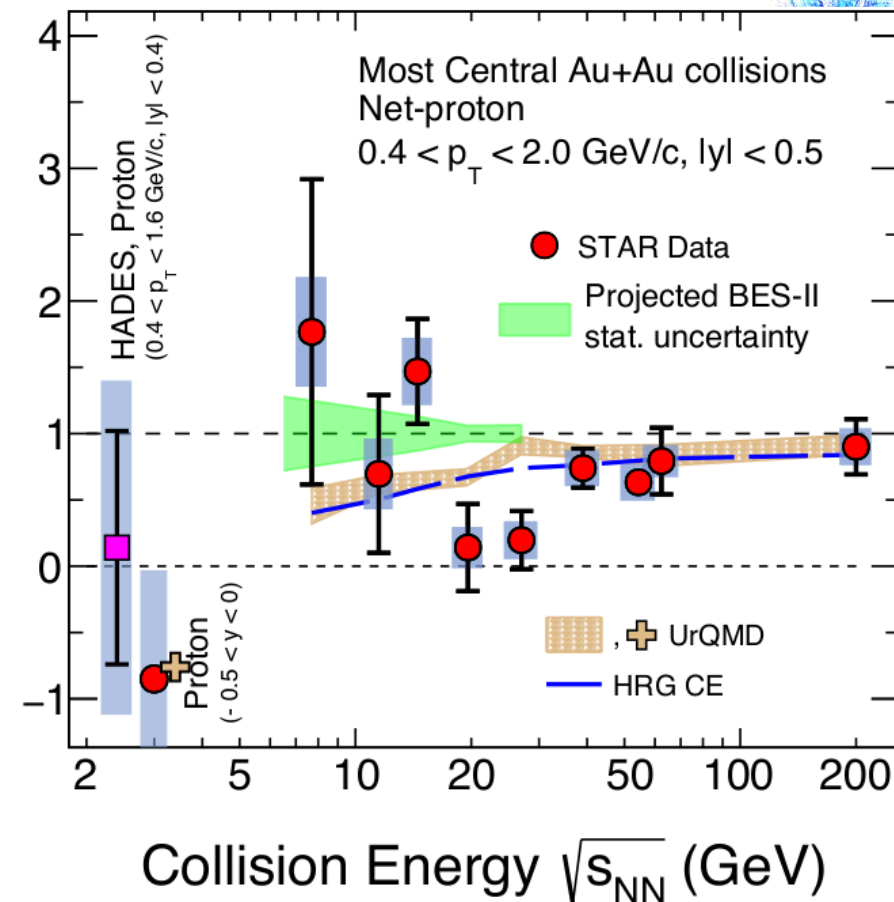
$$C_4 = \langle (\delta N)^4 \rangle - 3 \langle (\delta N)^2 \rangle^2$$

Moments

$$M = C_1, \sigma^2 = C_2, S = \frac{C_3}{(C_2)^{3/2}}, \kappa = \frac{C_4}{(C_2)^2}$$

$$\frac{C_2}{C_1} = \frac{\sigma^2}{M} \quad \frac{C_3}{C_2} = S\sigma \quad \frac{C_4}{C_2} = \kappa\sigma^2$$

Net-proton $\kappa\sigma^2$

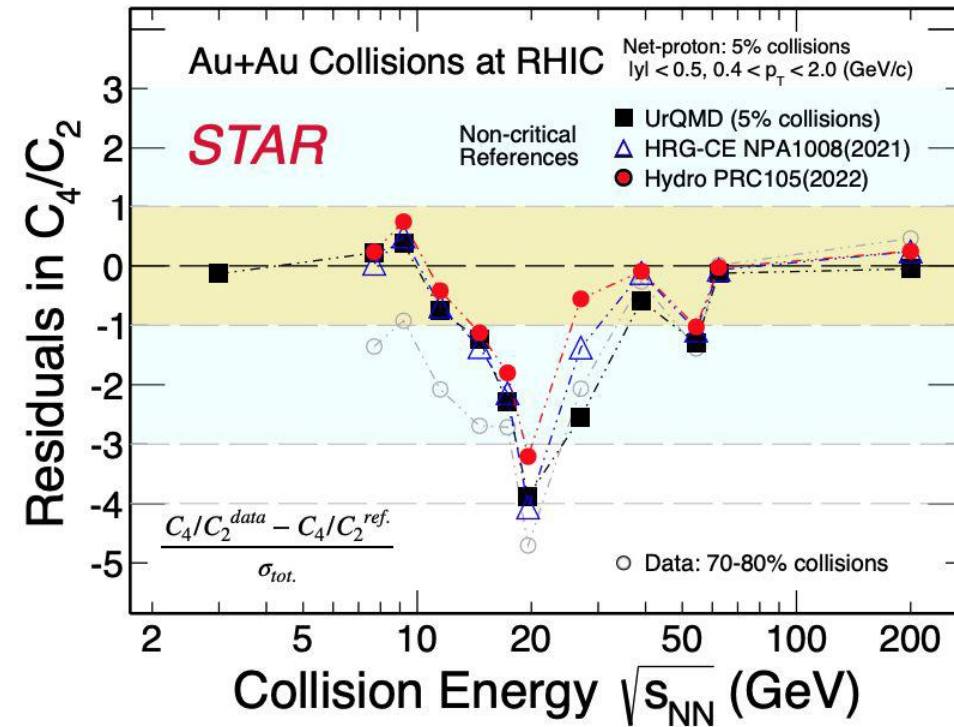
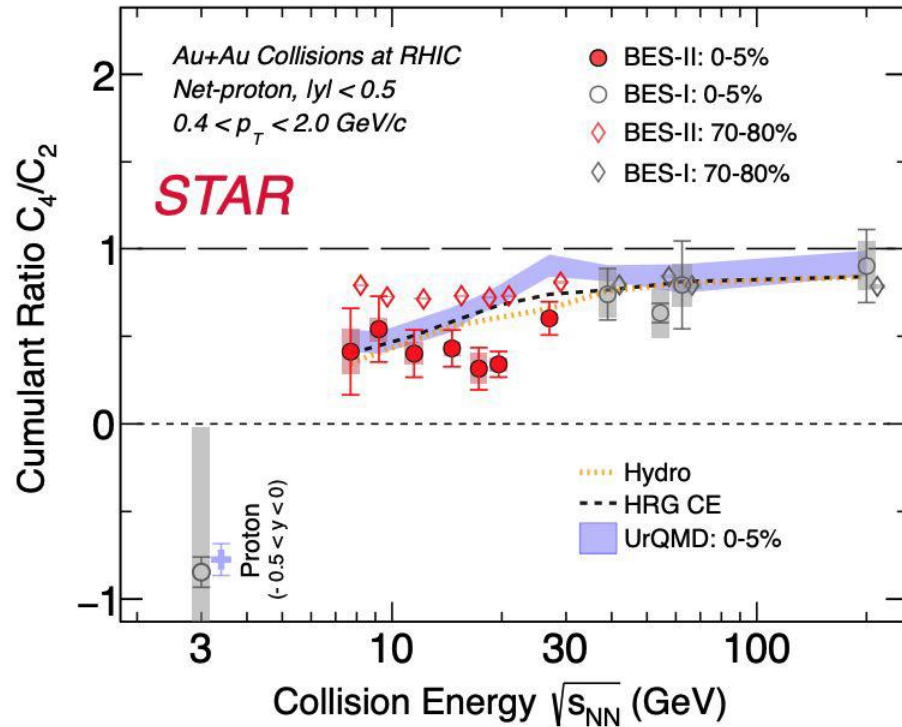


BES-I results showed a hint of fluctuations in the net-proton data but with high uncertainties

Net-proton cumulant measurements at STAR



non-monotonic behavior expected around critical point

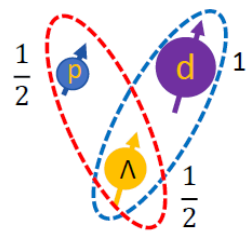


C_4/C_2 shows minimum around ~ 20 GeV comparing to non-CP models, 70-80% data
 Maximum deviation: $3.2 - 4.7\sigma$ at $\sqrt{s_{NN}} = 19.6$ GeV ($1.3 - 2.0\sigma$ for BES-I)

p-Λ and d-Λ Correlation Measurement in 3 GeV Au-Au collisions



Scatterings Length (f_0) and Effective Range (d_0)

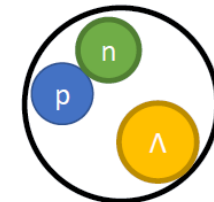


$$\frac{1}{f(k)} \approx \frac{1}{f_0} + \frac{d_0 k^2}{2} - ik$$

❖ The constraint of the effective range (d_0) is weaker

${}^3\Lambda\text{H}$ binding energy (B_Λ):

❖ Bethe formula from Effective Range Expansion (ERE) parameters $f_0(D)$ & $d_0(D)$

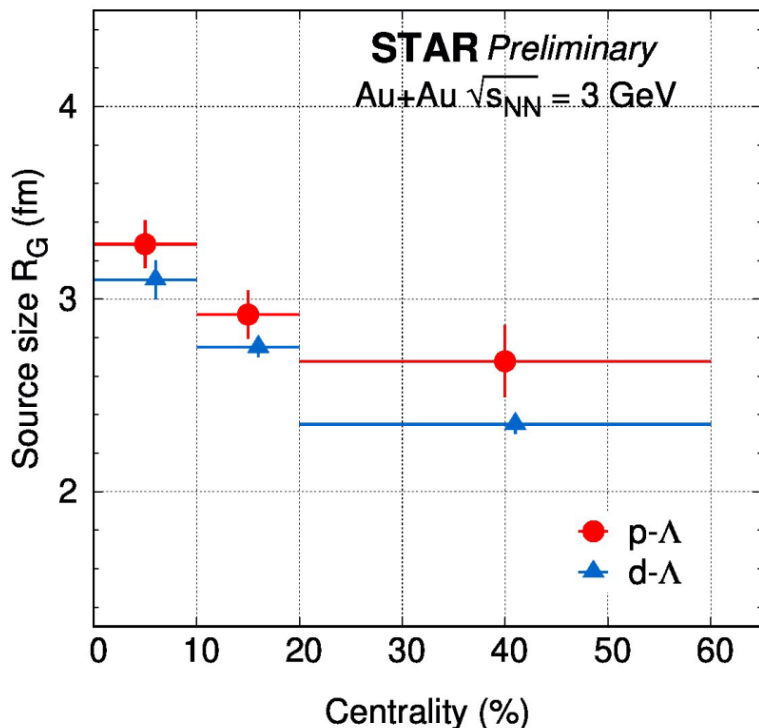


$$\frac{1}{-f_0} = \gamma - \frac{1}{2} d_0 \gamma^2 \quad \text{❖ } B_\Lambda = \frac{\gamma^2}{2\mu_{d\Lambda}}$$

❖ $\mu_{d\Lambda}$: reduced mass

❖ γ : binding momentum

Source Size with L-L approach

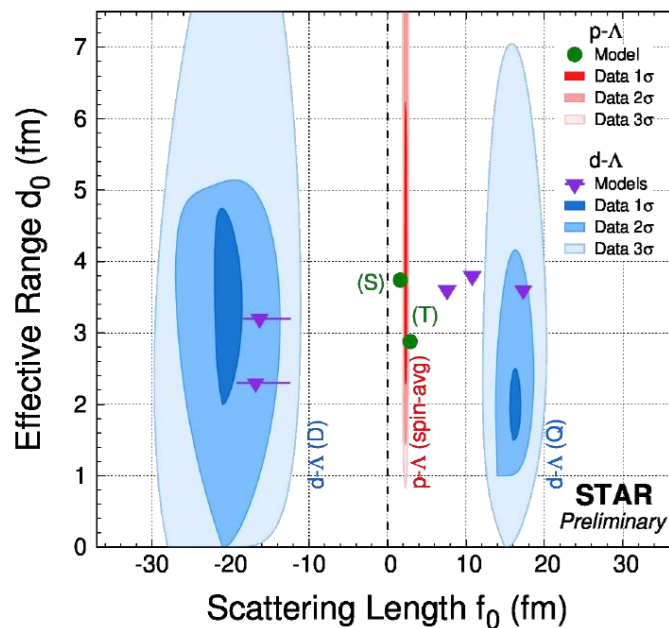


R_G : spherical Gaussian source of pairs by Lednicky-Lyuboshits (L-L) approach

- Separation of emission source from final state interaction

Collision dynamics as expected:

$$R_G^{\text{central}} > R_G^{\text{peripheral}} \quad \text{and} \quad R_G(p-\Lambda) > R_G(d-\Lambda)$$



p-Λ correlation spin-ave:

$$f_0 = 2.32^{+0.12}_{-0.11} \text{ fm}$$

$$d_0 = 3.5^{+2.7}_{-1.3} \text{ fm}$$

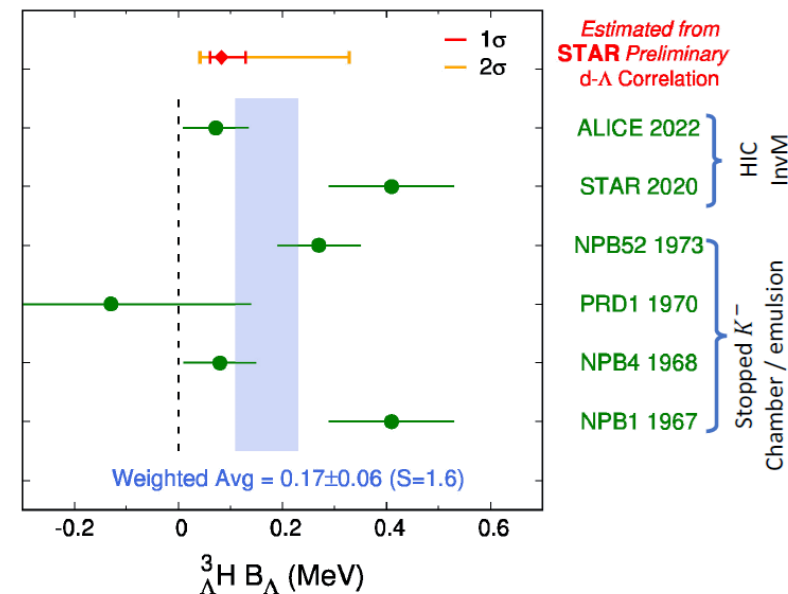
d-Λ correlation spin-sep:

$$f_0(D) = -20^{+3}_{-3} \text{ fm}$$

$$d_0(D) = 3^{+2}_{-1} \text{ fm}$$

$$f_0(Q) = 16^{+2}_{-1} \text{ fm}$$

$$d_0(Q) = 2^{+1}_{-1} \text{ fm}$$



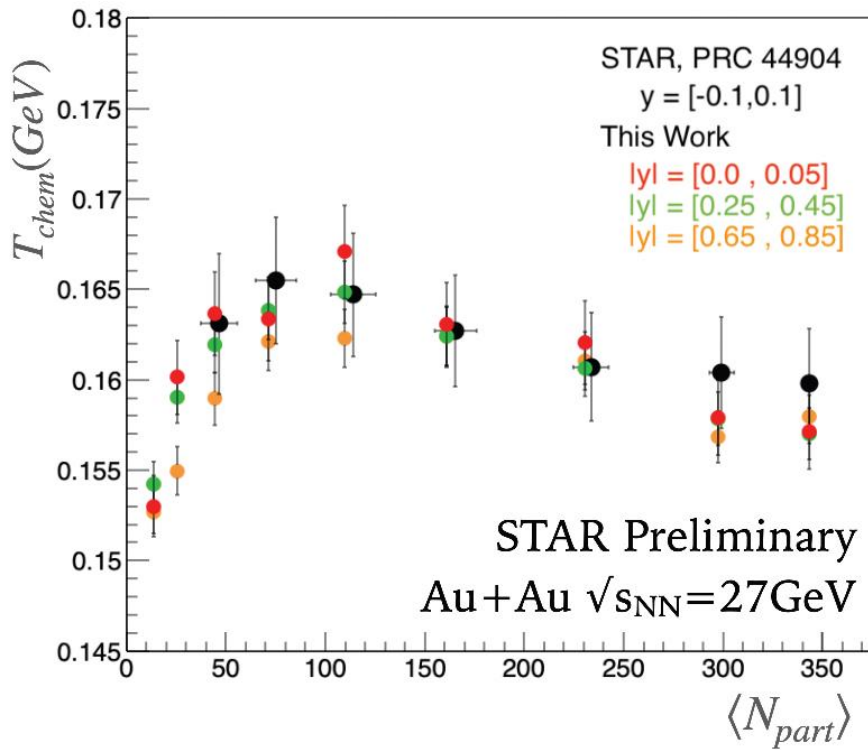
$${}^3\Lambda\text{H } B_\Lambda = [0.04, 0.33] \text{ (MeV) @ 95\% CL}$$

Consistent with the world average

Thermodynamical properties of the medium

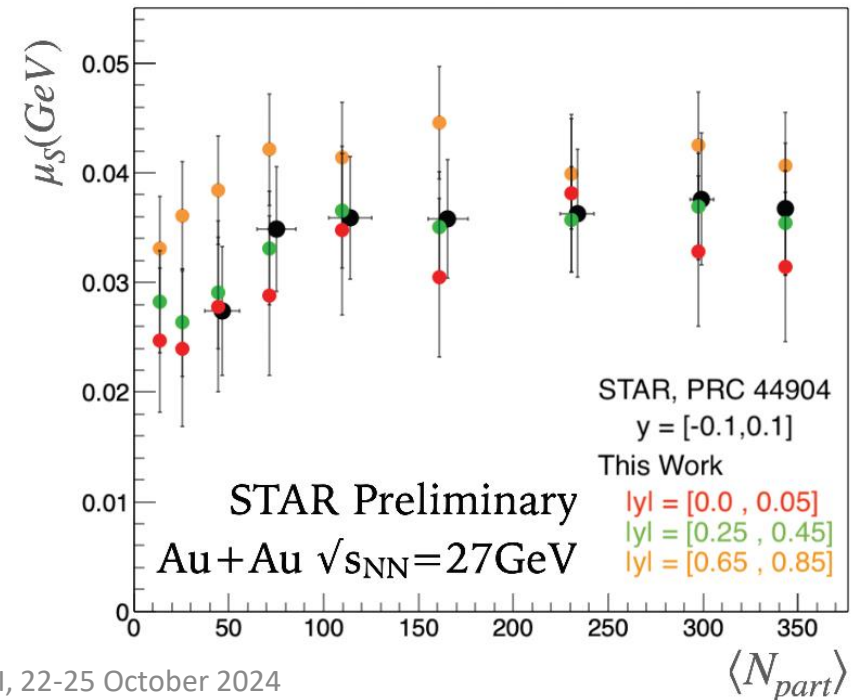
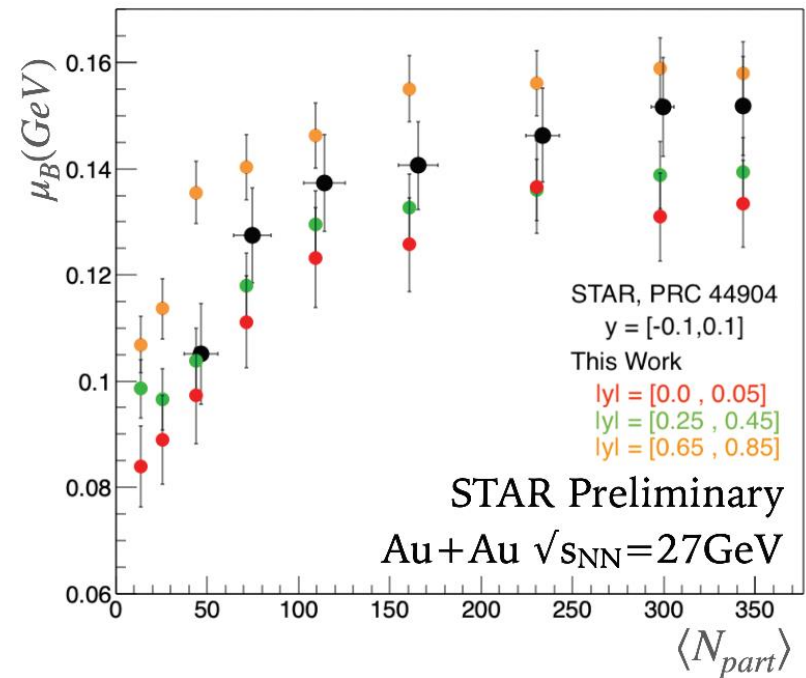


Precise study of the QCD phase diagram location of the freeze-out parameters at different collision energies

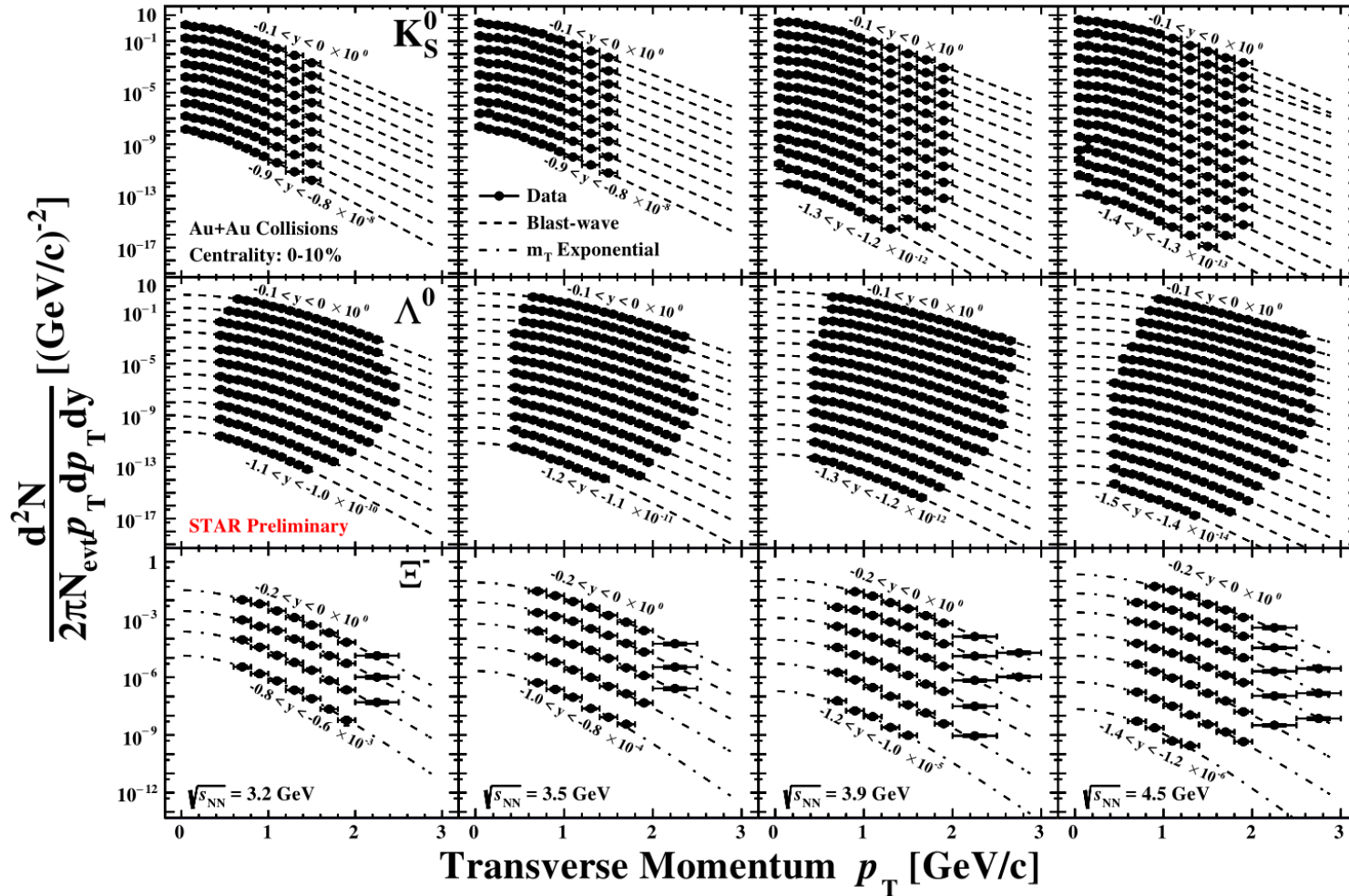


Fits by THERMUS
Chemical equilibrium
model

$\Delta\mu_B \approx 25\text{ MeV}$ for
 $\Delta y = 1$ at 27 GeV



Strange particle production near threshold



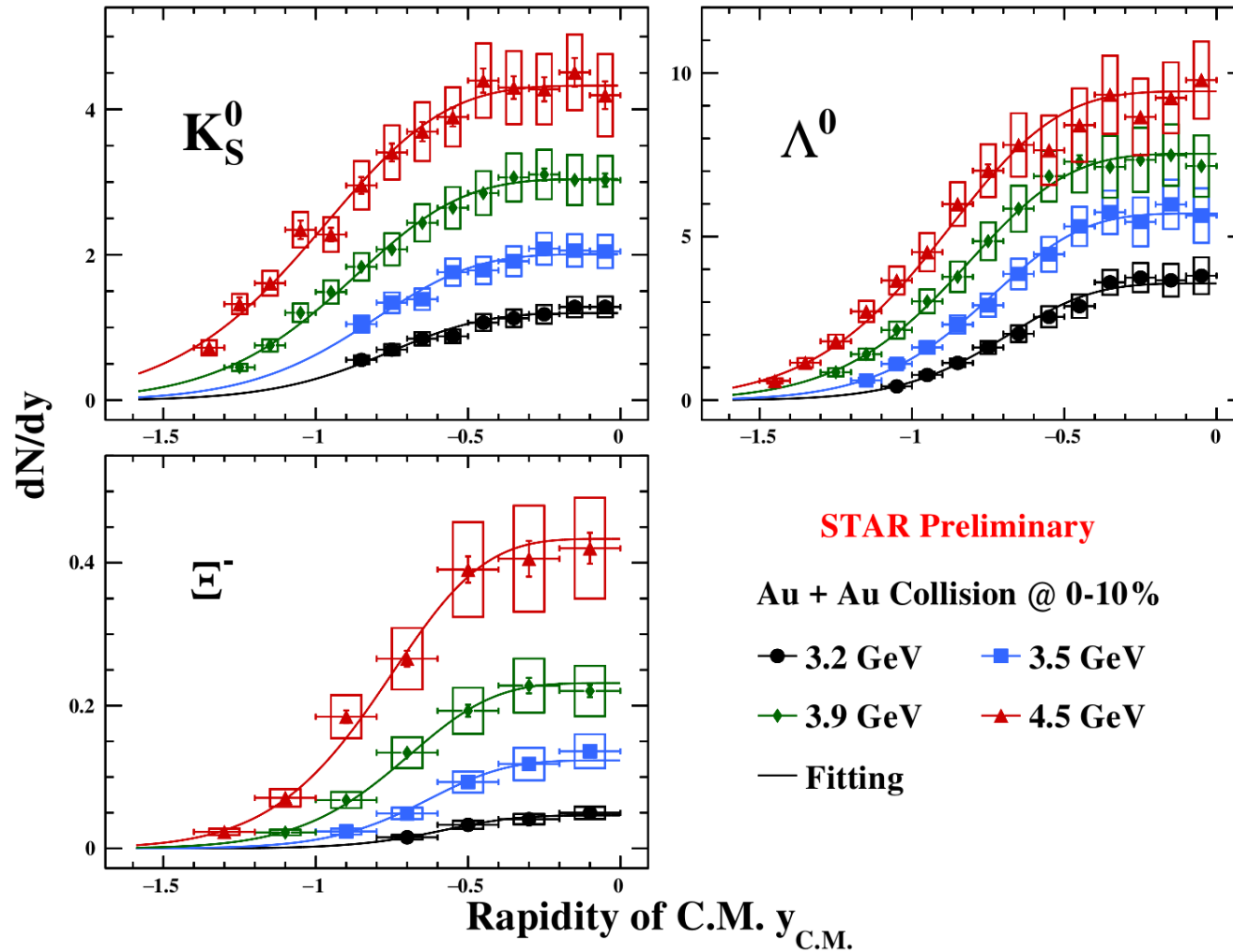
K_s^0, Λ, E^- transverse momentum spectra at FXT energies

Blast-wave fit for K_s^0, Λ

$$\frac{d^2N}{2\pi p_T dp_T dy} \propto \int_0^R r dr m_T I_0 \left(\frac{p_T \sinh \rho(r)}{T} \right) \times K_1 \left(\frac{m_T \cosh \rho(r)}{T} \right)$$

m_T exponential fit for E^-

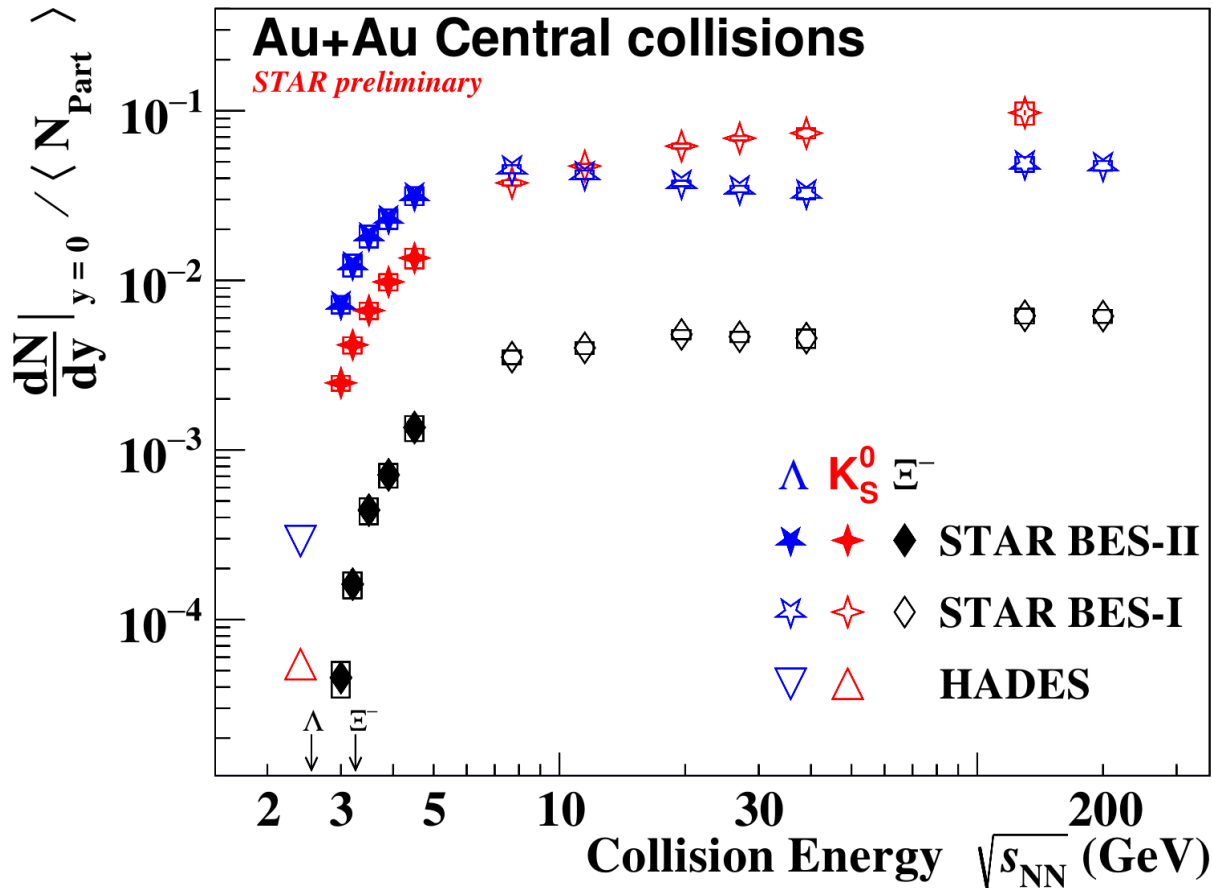
Rapidity dependence of strange particle production



Fitting function for dN/dy

$$\frac{dN}{dy} \sim \frac{1}{\text{Cosh}\left(\frac{y^2}{2\sigma^2}\right)} = \frac{2}{e^{\frac{y^2}{2\sigma^2}} + e^{-\frac{y^2}{2\sigma^2}}}$$

Strangeness production excitation function



Rich structure in strangeness excitation functions

➤ Production mechanisms are different at low and high energies (high and low baryon density)

Partonic interaction (pair production)

$gg \rightarrow ss$ or $qq \rightarrow ss$

Hadronic interaction (associated production)

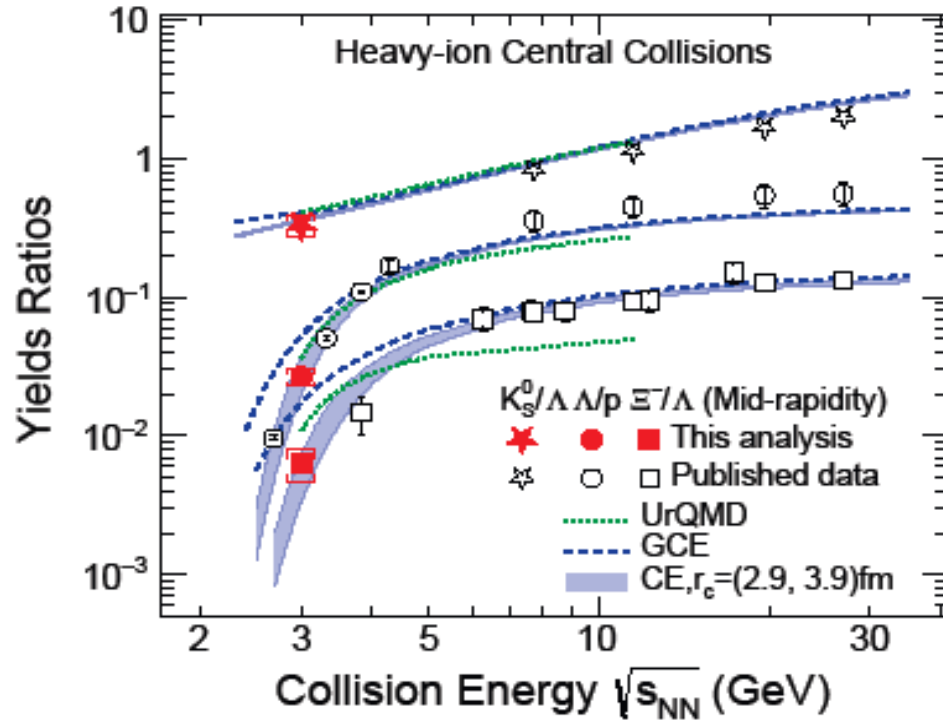
$BB \rightarrow BYK$ or $BB \rightarrow BEKK$

B: N, p, Δ , etc. Y: Λ , Σ , etc. K: K^+ , K^0

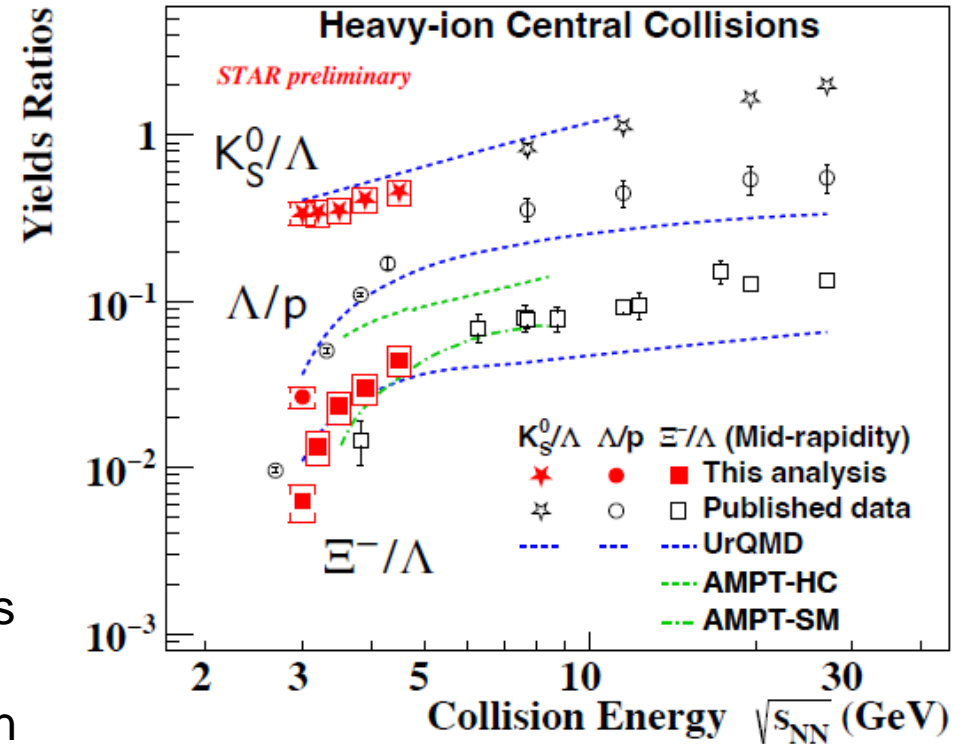
➤ Baryon-dominated to meson-dominated transitions
 K_S^0 and Λ mid-rapidity yield cross at ~ 8 GeV

➤ First measurement of Ξ^- near- / sub-threshold energies in Au+Au collision

Strange hadron yield ratios



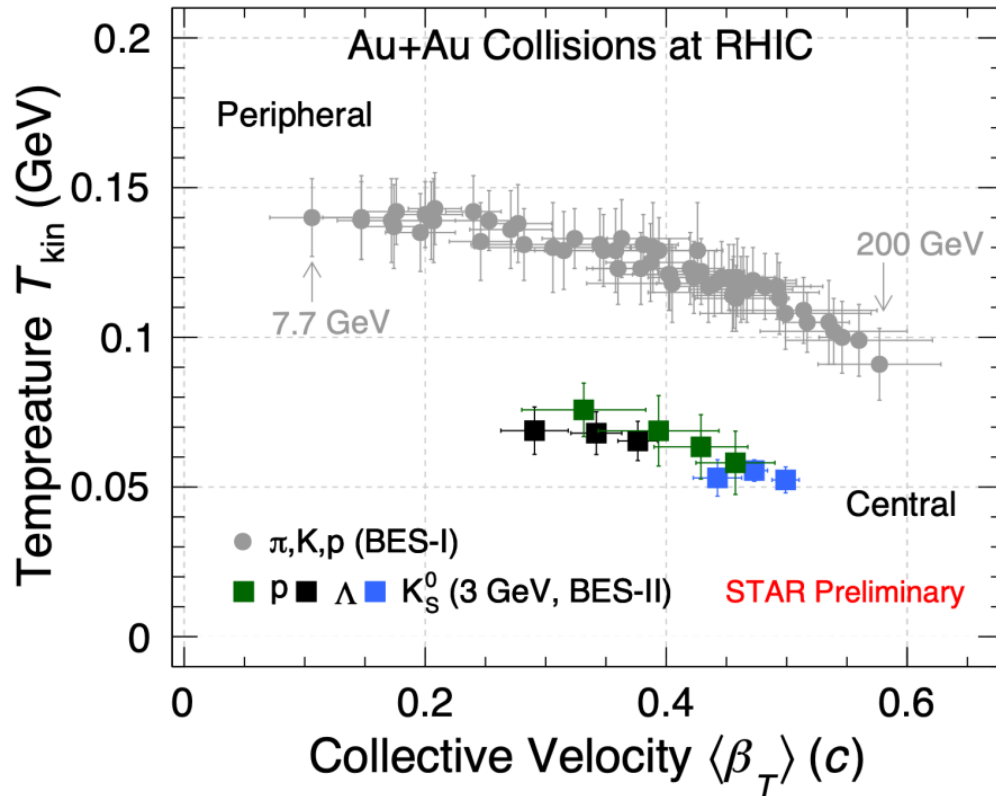
UrQMD and AMPT models cannot describe all data
 Strange baryons, especially for the double strangeness Ξ^- , are sensitive probes to the medium properties



Grand Canonical Ensemble (GCE) fails at low energies
 Canonical Ensemble (CE) with strangeness correlation length $r_c = 2.9 - 3.9$ fm simultaneously describes ratios at all energies

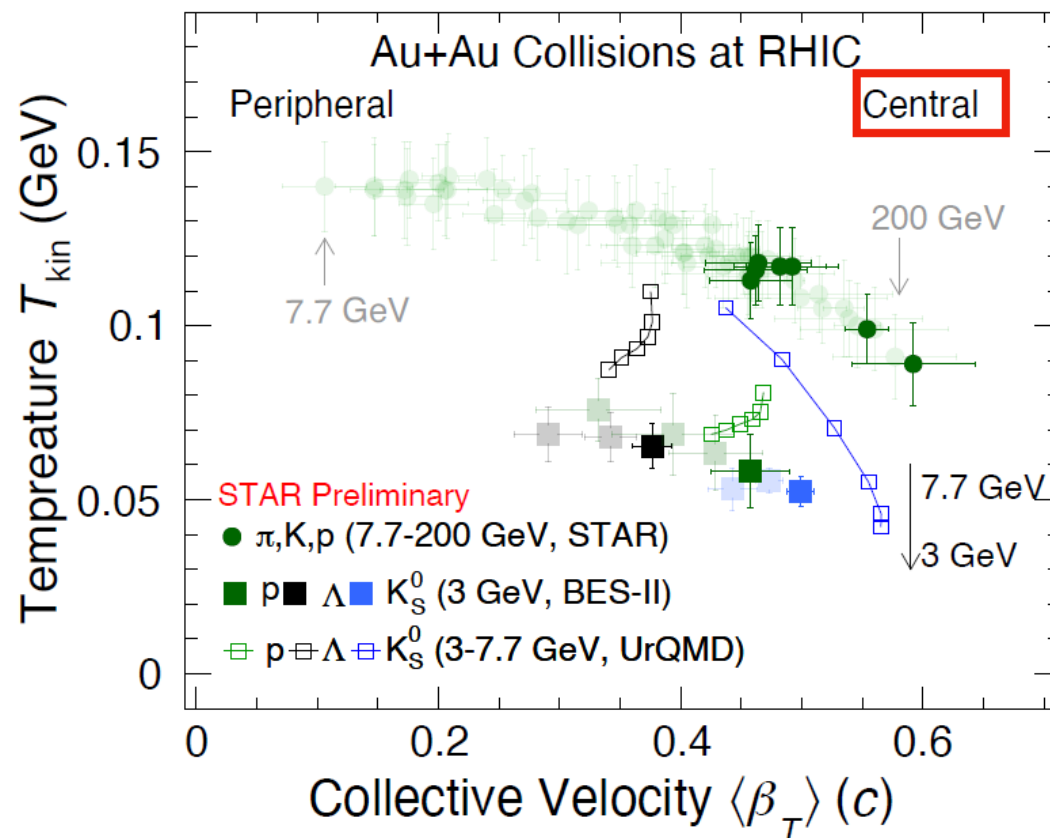
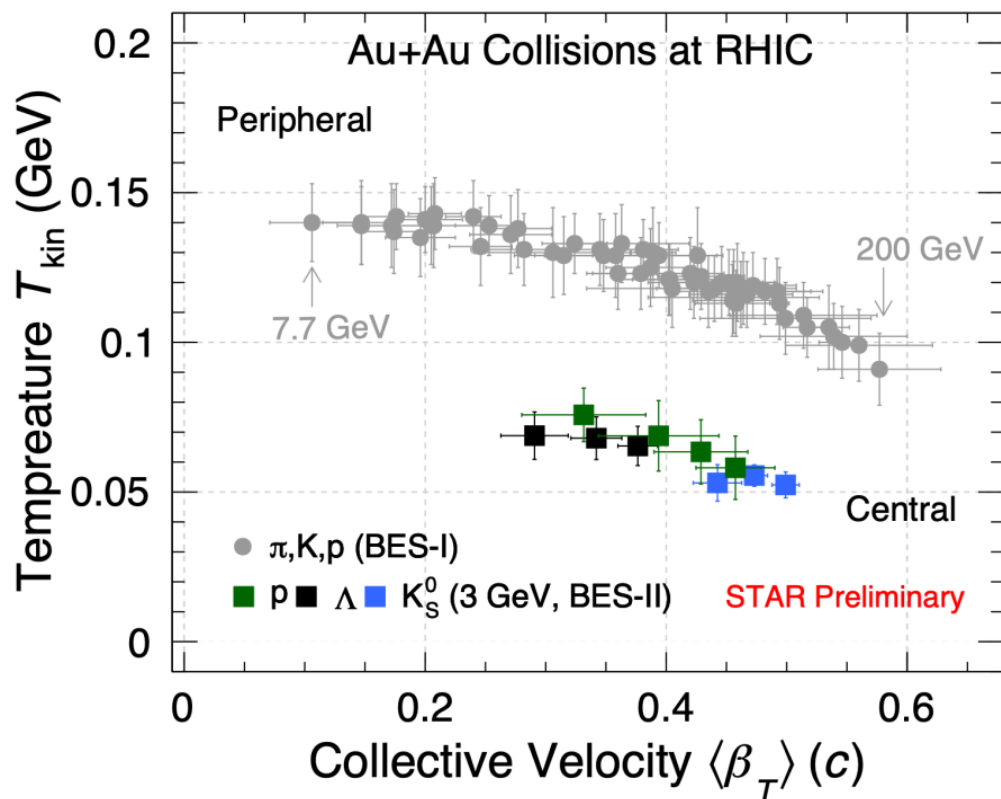
Change of medium properties at the high baryon density region

Kinetic free-out parameters at low collision energies



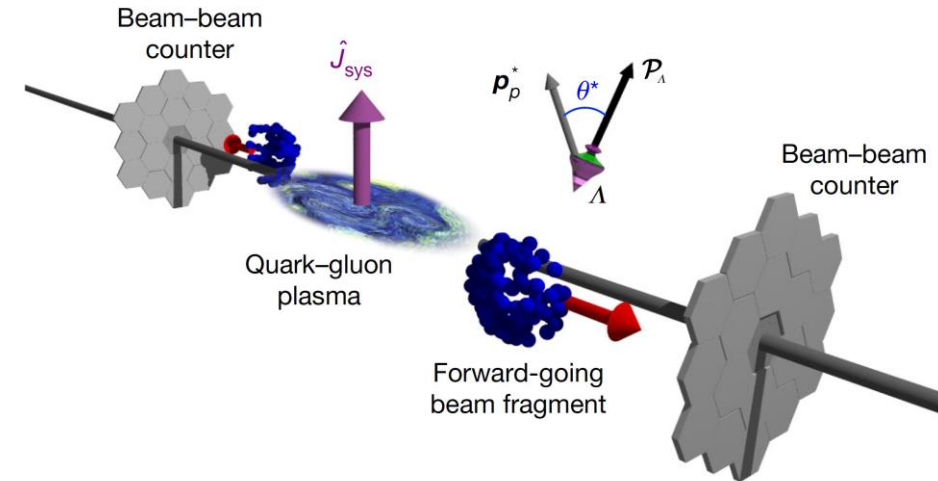
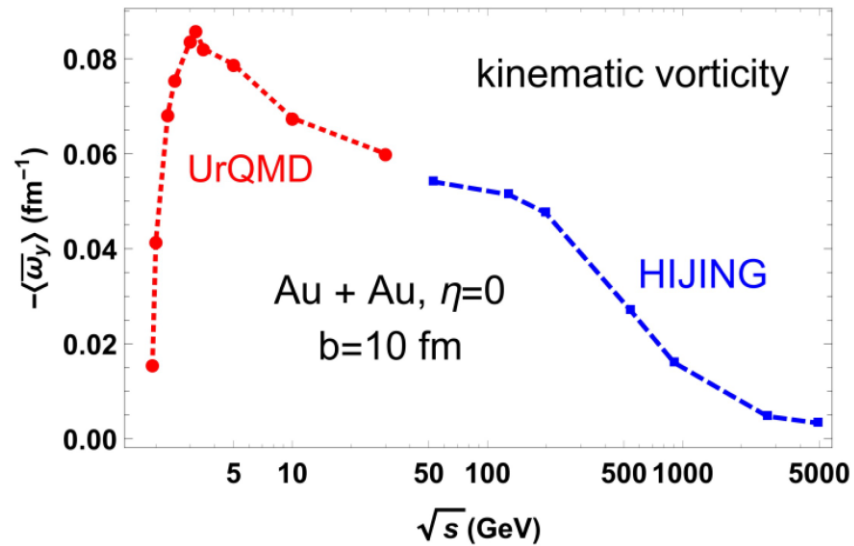
Kinetic parameters temperature T and velocity v extracted from the Blast-wave model are much different between 3 GeV and higher collision energies

Kinetic freeze-out temperature



Change in medium properties (EOS) or expansion dynamics

Vorticity and polarization



Orbital angular momentum

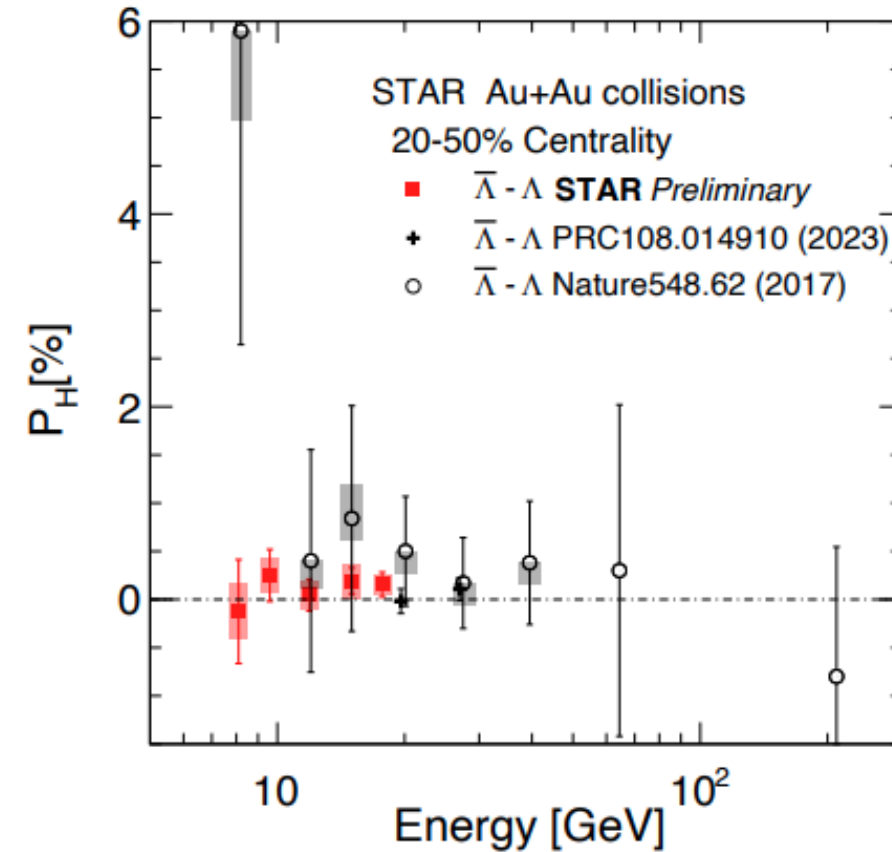
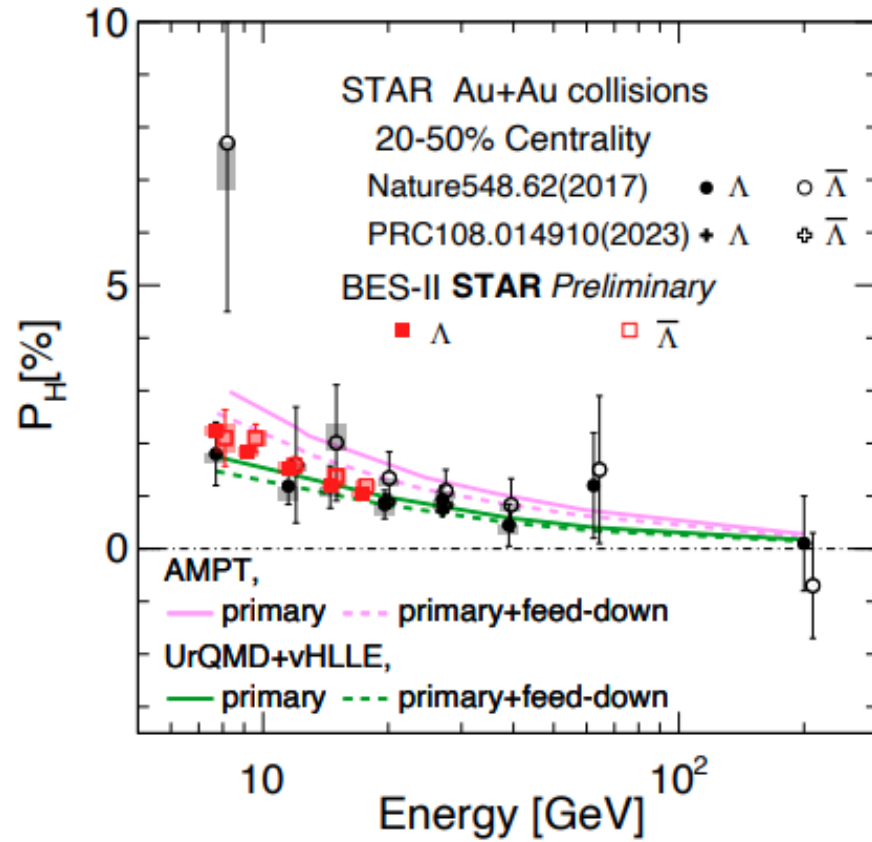
Local fluid vorticity $\omega = 1/2 \nabla \times v$

Leads to global polarization
along L though spin-orbit coupling

Self-analyzing, parity-violating weak decay channel of hyperons

Daughter baryon is preferentially emitted in the direction of the hyperon spin

Global Λ polarization



High precision measurements of global lambda polarization demonstrates no splitting between lambda and antilambda

Summary



STAR has collected large amounts of data at 7 collider and 13 fixed target energies in the energy range $\sqrt{s_{NN}}$ from 3 to 54.4 GeV where transition from hadronic to quark-gluon degrees of freedom is expected

Particle production at low collision energies demonstrates change in the kinetic freeze-out temperature

Breaking of the NCQ-scaling of elliptic flow is observed below 3.2 GeV and gets progressively restored with increase in collision energy

New precise measurements of the net-proton cumulant ratios has demonstrated deviation from model calculations without critical point at 19.6 GeV at the level 3.2 – 4.7 σ

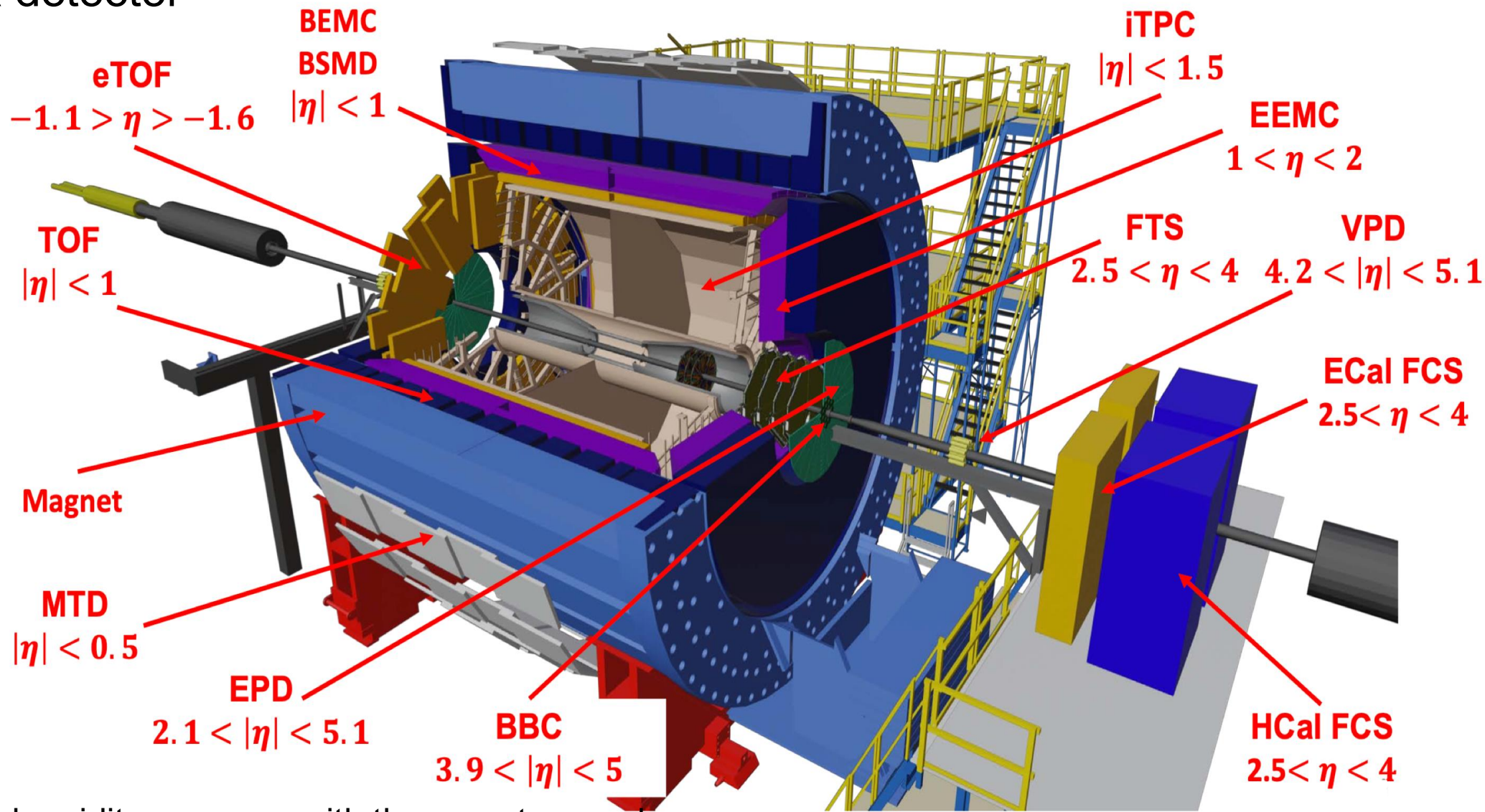
Precise measurements of Λ global polarization showed no significant difference between particles and antiparticles



Thank you for the attention!

Part of this work has been supported by Russian Science Foundation under grant № 22-72-10028

STAR detector



Extended rapidity coverage with the recent upgrades
Improved detector plane resolution
Improved particle identification capabilities

